

# Internal and effective stresses in high-temperature creep evaluated from transient dip tests and dislocation bowing

F. GROISBÖCK, F. JEGLITSCH

*Institut für Metallkunde und Werkstoffprüfung, Montanuniversität Leoben, A-8700 Leoben, Austria*

Because creep of metals and alloys is modelled on the basis of microstructural observations, it has been shown that there is a difference between the mathematical treatment of high-temperature deformation and the real material behaviour. One idea to consider is to split the applied stress into a part depending on the substructure (the internal stress which has to be reached to start dislocation motion) and a part describing the resistance to the glide motion of dislocations (the effective stress). For ferritic chromium steel these quantities have been measured by means of the stress transient dip test technique. This leads to mean values of internal and effective stresses for the whole specimen. Additionally, local stresses acting on individual dislocations are evaluated from dislocation bowing for a wide range of applied stresses. The results show that the ratio of internal to applied stress decreases with increasing applied stresses, which, on the other hand, causes a large increase of effective stresses. Dislocation bowing stresses show a similar dependence. Compared to the results of dip tests, the determination of local stresses leads to less accurate results and to a large deviation of results within small regions of one specimen. Therefore, it is only valuable for comparison purposes.

## 1. Introduction

High-temperature steady-state creep of crystalline materials is generally assumed to be controlled either by climb of edge dislocations (as occurs in pure metals) or by drag-controlled dislocation glide (as occurs in some alloys, e.g. Al–Mg). Various models (see, for example, Blum [1]) for these two micromechanisms of power-law creep lead to the so-called “natural” law of creep describing the creep rate,  $\dot{\epsilon}$ , as a function of stress,  $\sigma$ , and absolute temperature,  $T$

$$\dot{\epsilon} = A_1 (Dgb/kT) (\sigma/G)^n \quad (1)$$

The creep exponent,  $n$ , is 3,  $D$  is the coefficient of self-diffusion,  $G$  is the shear modulus,  $b$  is the length of the Burgers vector,  $k$  is the Boltzmann constant and  $A_1$  is a constant of the order 0.5 [2]. However, with many materials the natural creep law seems to be in conflict with experimental results [2]. In a wide range of stresses, nearly all pure materials and most single-phase alloys show creep exponents,  $n$ , between 4 and 10 but power-law creep is still working [3]. This is thought to be a consequence of the variation in the substructure of the materials, which occurs during creep deformation.

If the influence of the substructure on deformation behaviour and thus on the creep exponent,  $n$ , is to be considered, it is useful to apply the concept of internal and effective stresses [2]. The applied stress,  $\sigma$ , is assumed to be the total of an internal stress,  $\sigma_i$ , and an

effective stress,  $\sigma_e$

$$\sigma = \sigma_i + \sigma_e \quad (2)$$

$\sigma_i$  rises because of the inhomogeneity of the substructure (subgrain and cell walls, immobile dislocations) [4] and acts against the dislocation motion. This stress must be supplied before dislocations become mobile.  $\sigma_e$  describes that part of the applied stress which forces the dislocation motion through the obstacle-free matrix, an effect similar to friction hindering the sliding of a macroscopic body.

Pure metal power-law creep is modelled with a very low effective stress [2]. The model is approximately valid in many materials when the temperature is high and the applied stress is low [5]. Experimental results show that under these deformation conditions the creep exponent,  $n$ , reaches values near 3 [5].

At very high stresses and low temperatures, respectively, the deformation mechanism is exponential creep (often called “power-law breakdown”), which is thought to be the thermally activated but diffusionless glide process of the dislocations [2]. Although theories show that the creep rate should increase exponentially with increasing stress [2], experimental results are often fitted to the power-law relation (Equation 1). This leads to very high creep exponents,  $n$  (up to 50 [6, 7]). As exponential creep leads to a more homogeneous dislocation distribution (cell structure or regions with homogeneously distributed

dislocations [6, 7]) than can normally be observed in power-law creep [6], the resultant  $\sigma_i/\sigma$  value is narrower than in the power-law region [2].

Far below the transition to the mechanism of exponential creep, the ratio of  $\sigma_i/\sigma$  begins to deviate from unity [8], leading to a deviation of experimental results from theory and thus to a continuous increase of the creep exponent,  $n$ . Much work was done to determine internal and effective stresses for a large number of materials under various deformation conditions (see, for example, the report of Takeuchi and Argon [8]), but only a few researchers correlated measured effective stresses to the resulting strain rates, which normally leads to creep exponents as they are predicted by the models of power-law creep (see [9, 10]). Nowadays, creep behaviour is usually modelled in terms of dislocation velocity by combining constant structure creep data (e.g. from stress relaxation experiments) with the variations of substructure which are described by  $\sigma_i$  and  $\sigma_e$  [11]. The advantage of the latter method is that it is possible to determine various influences on dislocation motion and thus on the micromechanism of creep with a higher accuracy. However, irrespective of what should be done, it is necessary to determine internal and effective stresses.

Internal stresses are mechanically measurable by means of the so-called transient dip tests [12, 13]. The stress applied to a creeping specimen is reduced to a varying extent. When the remaining stress equals the mean long-range internal stress, a zero creep rate is obtained after the stress reduction. A transmission electron microscopical (TEM) analysis of the substructure also offers the possibility to evaluate the height of local internal and effective stresses. This can be done by measuring the dislocation curvature [14]. Although this method will not always provide very exact data, it is useful to check the distribution of internal stresses within the substructure.

The aim of this work is to present results on internal and effective stresses for a ferritic steel obtained by means of the dip test technique. The same quantities are evaluated from transmission electron micrographs by measuring dislocation curvature. The results are discussed in terms of accuracy and applicability for modelling deformation.

## 2. Experimental procedure

The material investigated was ferritic chromium steel X10CrAl 18, with the composition shown in Table I. To check the influence of grain and carbide size on the creep behaviour, two structural states of the material were tested. The final step in the fabrication process of the so-called conventional (con.) material was to roll the material at a temperature of about 1000°C to a section of 20 mm × 20 mm, subsequently cooling it in

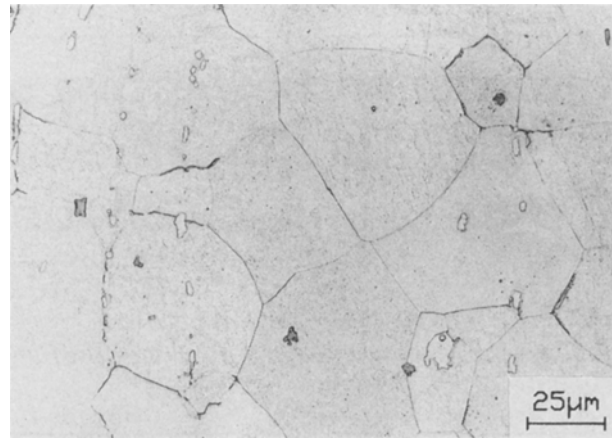


Figure 1 Grain and carbide structure of the alloy X10CrAl 18 in the conventional condition.

static air. This produces equiaxed grains with a size of about 50  $\mu\text{m}$  and large carbides (1–20  $\mu\text{m}$ ). Fig. 1 shows a typical section parallel to the rolling axis of the conventional material.

The modified (mod.) material was first rolled to a diameter of 30 mm, then solution treated (1 h at 1200°C) and subsequently subjected to a water quench to keep the carbon in supersaturated solid solution. The rods were then forged to a diameter of 20 mm at about 700°C. Finally, a recrystallization treatment (1/2 h, 880°C) with subsequent water quench was applied. Two typical optical micrographs of the modified material are shown in Fig. 2a and b. Fig. 2a shows a section parallel to the longitudinal axis of the rods. Because of bad etchability of the grain boundaries built during the last heat treatment (recrystallization), Fig. 2a shows only an incomplete view of the grain structure. Fig. 2b shows some “disappearing” grain boundaries (see arrows) which make the determination of grain size difficult and uncertain. An approximated value for the grain size was obtained by counting in the sections between grain boundaries and the edge of the large hole in a TEM foil. With this method an average grain size of about 10  $\mu\text{m}$  was obtained. The carbide size of the modified material was 0.1–1  $\mu\text{m}$ . The largest carbides were found at the original (solution treated) grain boundaries. The carbide size in the grain interiors is near 0.1  $\mu\text{m}$ . The carbide distribution can be seen from Fig. 2b.

Mechanical testing (creep tests, stress relaxation tests and stress transient dip tests) was done in the temperature range 500–750°C and at strain rates of  $2 \times 10^{-7}$  to  $2 \times 10^{-2} \text{ s}^{-1}$ . The temperature was kept constant within an interval of  $\pm 3^\circ\text{C}$  over time and length of the specimen. Most of the creep tests and all of the relaxation and dip tests were applied on an

TABLE I Chemical composition of the investigated ferritic steel X10CrAl 18 (wt %)

C	Si	Mn	P	S	Cr	Mo	Ni	W	Cu	Al
0.09	1.19	0.45	0.024	0.013	17.75	0.03	0.30	0.01	0.13	1.09

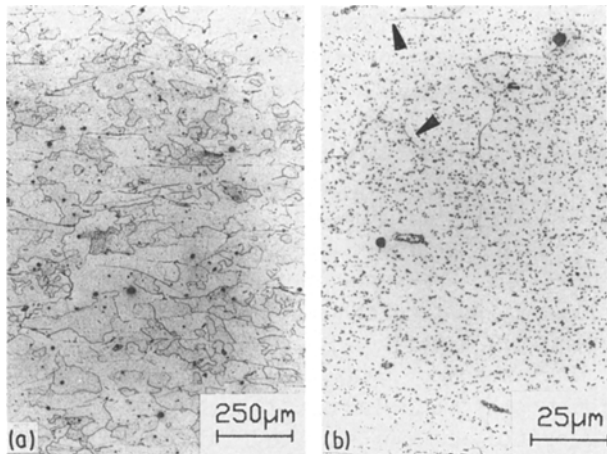


Figure 2 Grain and carbide structure of the alloy X10CrAl 18 in the modified condition. (a) Grain structure, (b) carbide distribution; arrows indicate "disappearing" grain boundaries.

Instron-type testing machine. Deformation is transferred outside the furnace with two pairs of rods and measured with a LVDT transducer with an accuracy better than  $10^{-4}$ .

Stress transient dip tests were applied to measure internal stresses. With these tests stress reductions of different magnitudes are applied after the specimen had been crept to a desired condition (well into the steady state). All specimens subjected to substructural investigations were crept to a deformation of  $\epsilon \approx 0.2$  and then cooled under load to prevent recovery of dislocation structures during the cooling period. These structures were analysed in the TEM. Most of the foils were taken from a plane perpendicular to the applied stress but some were cut from a plane parallel to the stress axis. At high stresses (near the transition to and in the exponential creep region) small elongations of subgrains and cells in the stress direction can be found. It is assumed that this elongation does not have a large influence on the bowing of dislocations and therefore on the results of local stresses. Thin platelets about 0.3 mm thick were cut and then ground under water cooling in several steps to a thickness of about 50  $\mu\text{m}$ . Foils of 3 mm diameter were punched and then electrolytically polished (electrolyte 133 ml  $\text{CH}_3\text{COOH}$ , 25 g  $\text{CrO}_3$ , 7 ml  $\text{H}_2\text{O}$ ). Most of the carbides fall out during electrolytical preparation. This sometimes leads to relatively small transmissible regions.

### 3. Results and discussion of internal stress measurements

#### 3.1. Modified method for the evaluation of dip tests

Many experimental problems arise in connection with the interpretation and evaluation of dip tests. The most important is that the internal stress changes very rapidly to another level if the applied stress is altered. Even with fast machines a finite time is necessary for a stress reduction, therefore all test results are affected by recovery [15]. To overcome this problem, a new method for the evaluation of dip tests was developed.

At each level of applied stress about 10–20 experiments (stress reductions, most of them a little larger than the expected effective stress) are necessary. Fig. 3 is a schematic plot which shows how the actual stress (continuous line) varies with time after a stress reduction  $\Delta\sigma$  larger than  $\sigma_e$  (the actual stress is narrower than  $\sigma_i$ ). Immediately after stress reduction and the subsequent stopping of crosshead motion, the actual stress increases because of a plastic shortening of the specimen (the average dislocation motion is backwards due to a negative average effective stress), which must be balanced by a positive elastic strain (region 3 in Fig. 3).

If the stress applied after stress reduction is larger than the internal stress at that time, the actual stress decreases (Region 1). This is a consequence of a positive mean effective stress which leads to forward deformation. The specimen continues to elongate after the stress dip when a tensile stress is applied. Therefore, an elastic shortening of the specimen occurs. If the actual stress remains constant for a short time (Point 2) it is equal to the momentarily acting internal stress. At this point, the condition of a delay in overall plastic deformation, as originally proposed by Solomon [12] and Ahlquist and Nix [13], is fulfilled.

Owing to reorientation processes of the dislocation structure (recovery), the internal stresses decrease during and after the stress dip. Each actual stress–time curve with a stress decrease beneath the actual level of the internal stress can be divided into three characteristic regions which are plotted in a diagram of stress over time after the beginning of reduction. Fig. 4 gives an example for an applied stress of 165 MPa. Points

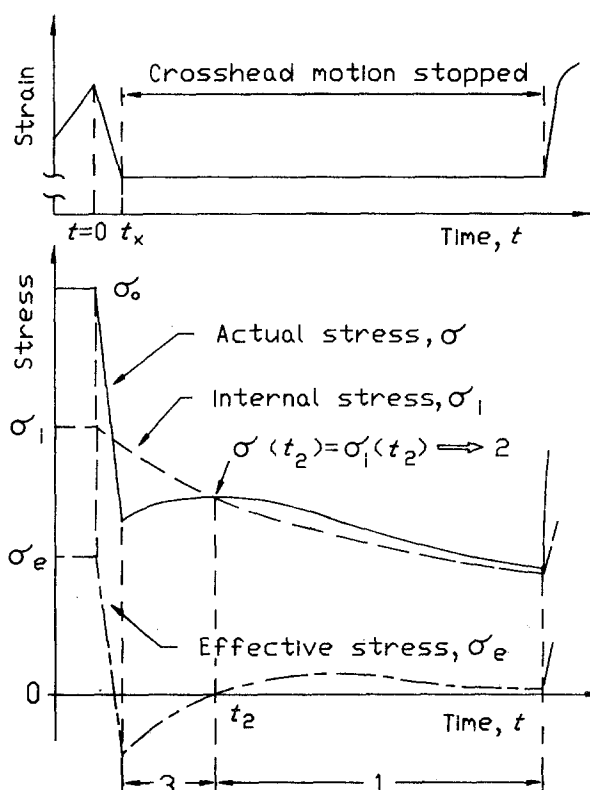


Figure 3 Schematic plot of time behaviour of applied stress,  $\sigma$ , internal stress,  $\sigma_i$ , and effective stress,  $\sigma_e$ , after a large stress reduction (stress transient dip test).

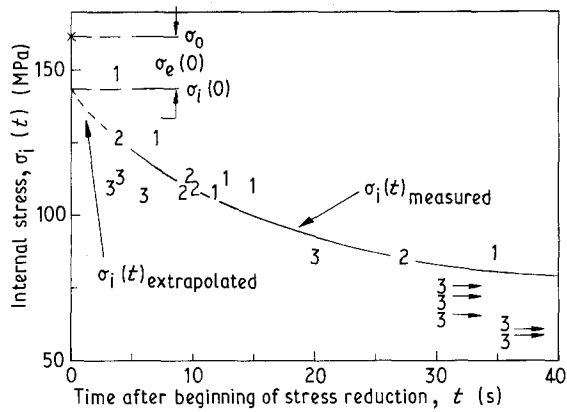


Figure 4 Example for the evaluation of a series of stress reductions from an original stress level of 165 MPa. 1, 2 and 3 correspond to Regions 1 and 3 and to Point 2 in Fig. 4, see text.

marked "2" correspond to internal stresses which are acting at different times. The time necessary for the actual stress to reach a constant value (Point 2, Fig. 3) decreases with decreasing negative effective stress (—, Fig. 4). An extrapolation (---, Fig. 4) to the beginning of stress reduction ( $t = 0$ ) leads to the internal stress at an applied stress of  $\sigma_0$ .

Points 1 and 3 are taken from Regions 1 and 3, respectively (see Fig. 3). They do not refer to internal stresses. These points are only used to control the interpolation and extrapolation. Points marked "1" indicate a decrease of two digits in load signal (which corresponds to a decrease of 0.16 MPa) after reaching the highest stress level. Points marked "3" with an arrow show that the actual stress is still increasing at the end of the reduction period. This means that during the reduction period the internal stress is always higher than the stress acting on the specimen. Other points marked "3" indicate that the stress is increasing at least one digit of load after the end of the stress dip.

This evaluation method makes it possible to eliminate the influence of recovery on the determination of internal stresses, except for such processes which have ended before the first measurements can be taken. The most important recovery process is the straightening of bowed dislocations under the reduced stress [16]. This may have a large influence in the case of pure metals and very soft solution-hardened alloys because there is no strong resistance to a fast glide process. If there are strong reaction forces between dislocations and foreign atoms (e.g. in Al-Mg alloys) dislocations cannot change their curvature during stress reduction to a certain amount. As shown elsewhere [6, 7, 17], the investigated material belongs to the group of alloys with strong reaction forces as long as it is deformed in the power-law creep region. In this case the evaluation method presented above is able to avoid systematic errors due to recovery. In the exponential creep region there is evidence that the interaction between dislocations and alloying atoms is small [7, 17]. Under these deformation conditions some small errors due to fast glide processes of dislocation cannot be excluded. Up to now, no other method could be found which avoids these errors.

### 3.2. Results of stress transient dip tests

The internal stress measurements with stress transient dip tests were performed at 600 °C for both material conditions. Fig. 5a shows the results for the modified material and Fig. 5b for the conventional material. The internal stress increases with increasing applied stress (continuous line) but the ratio  $\sigma_i/\sigma$  (---) decreases. Therefore a larger part of the applied stress forces the dislocation motion at higher applied stresses. The same has been observed for various metals, see, for example, [8, 15, 18].

In accordance with the well-established creep theory of Nix and Ilschner [2] (creep substructure is thought to consist of "hard" and "soft" regions, which means subgrain walls and subgrain interiors, respectively), the effective stress shows a very steep increase in the transition region to the exponential creep mechanism. This is a consequence of the ceasing increase of internal stress. It is well accepted that internal stress rises because of the inhomogeneity of the dislocation distribution [2, 4]. Fig. 6 shows a schematic plot of the stress distribution within a subgrain structure. The subgrain walls provide sites of very high dislocation density (e.g. for a subgrain misorientation angle of 1° [7, 8] a local dislocation density of about  $5 \times 10^{15} \text{ m}^{-2}$  can be calculated) and therefore of large

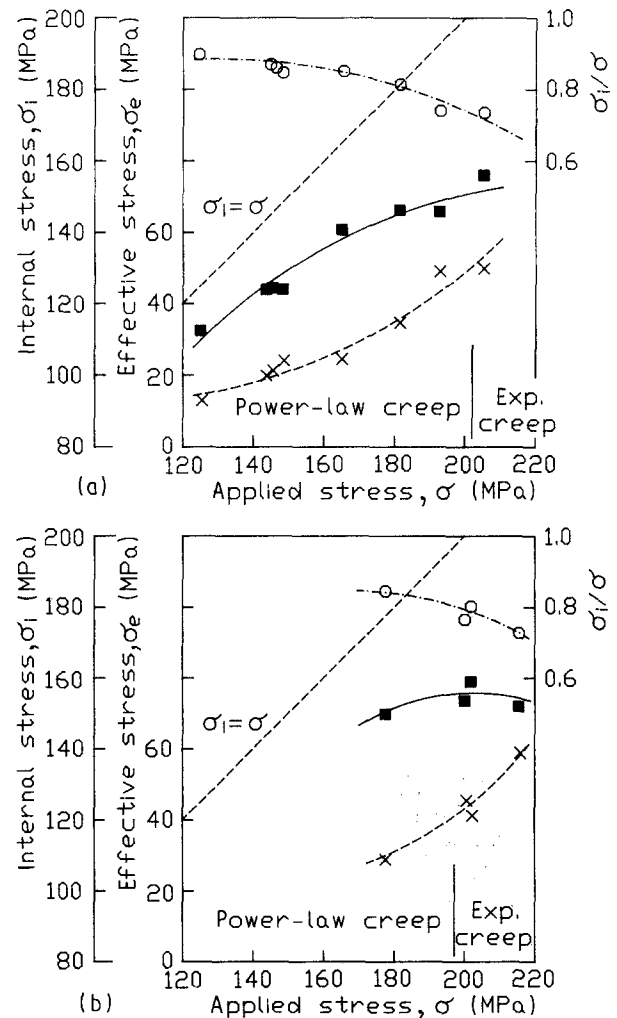


Figure 5 Results of stress transient dip tests at 600 °C, on (a) modified material, (b) conventional material. (■)  $\sigma_i$ , (×)  $\sigma_e$ , (○)  $\sigma_i/\sigma$ .

accommodation stresses. Long-range internal stresses are introduced to the surrounding subgrain interiors to keep balance with these high local stresses [2]. As the dislocation accumulation becomes less sharp when the substructure changes from subgrain to cell formation (as is the case at the transition from power law to exponential creep [6, 7]), the ratio of  $\sigma_i/\sigma$  decreases. This was also found to be true for the steel investigated.

### 3.3. Local stresses

A large number of specimens which were deformed to the steady-state conditions was analysed in the TEM. The local stresses,  $\sigma_i$ , acting on individual dislocation segments can be estimated from their radius [14]

$$\sigma_i = \alpha \frac{Gb}{r} \quad (3)$$

where  $\alpha$  is a constant factor for which Friedl [19, 20] uses values between 0.5 and 1,  $\sigma_i$  is shown in Fig. 6. As the stress,  $\sigma$ , is applied, the stress distribution shifts from the dashed to the continuous line. If a dislocation is, for example, fixed in intersection points with other dislocations, it bows between these pinning points [14]. It is assumed that all dislocations experience the full applied stress [14]. As the long-range internal stress,  $\sigma_i$ , is acting against the applied stress (Equation 2,  $\sigma - \sigma_i = \sigma_e$ ), the bowing stress,  $\sigma_i$ , corresponds to the effective stress,  $\sigma_e$ , acting on individual dislocations.

Problems arising from different orientation of dislocations to the foil plane are solved by approximating the radius of visible dislocation bows. If the glide plane of the dislocations is oriented at angles  $\alpha_1$  and  $\alpha_2$  to the foil plane (see Fig. 7a), a distorted picture of the dislocation bow will be seen. It is impossible to obtain a correct measure of the radius,  $r$ , without knowing  $\alpha_1$  and  $\alpha_2$ . To obtain suitable approximation, the radius of curvature is taken as the diagonal of a rectangle which is positioned around the dislocation bow with the longest side parallel to the flattest end of the bow

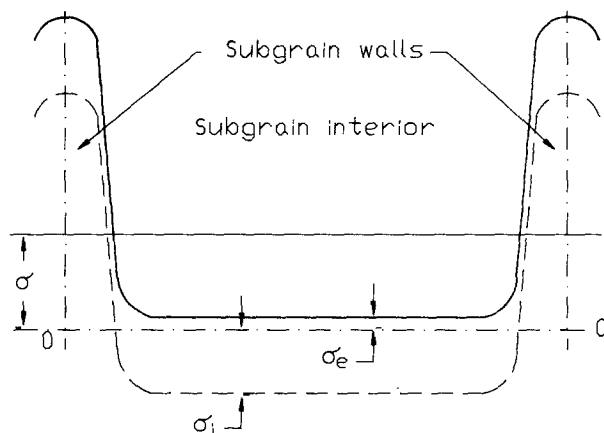


Figure 6 Schematic plot of stress distribution within a subgrain structure due to the model of Nix and Ilshner [2]. (---) Distribution of local stresses due to dislocation distribution without an applied stress,  $\sigma$ ; (—) shifted stress distribution with a superimposed stress,  $\sigma$ .

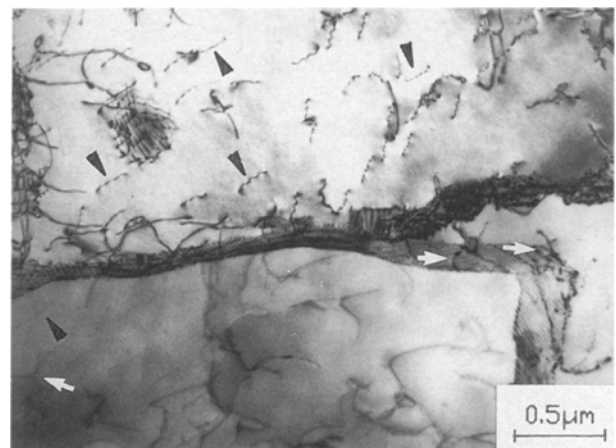
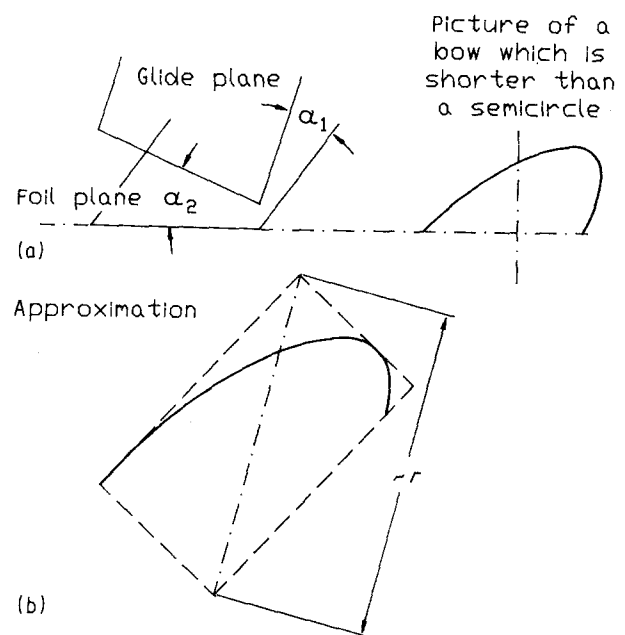


Figure 7 Arrangement of bowed dislocations and evaluation method for distorted bows. (a) Schematic plot of a dislocation bow oriented at the angles  $\alpha_1$  and  $\alpha_2 \neq 0$  to the foil plane. (b) Principle of the approximation method for the radius of distorted bows. (c) Substructure of a specimen crept at 160 MPa at 600°C (conventional material). White arrows show some strongly curved dislocations (some of them in the vicinity of subgrain boundaries), while black arrows indicate some soft-bowed dislocations.

(Fig. 7b). The error in  $r$  can be large if  $\alpha_1$  and  $\alpha_2$  are large (large distortion of the picture). Therefore, only slightly distorted pictures of dislocation bows were evaluated. The radius of a very slightly distorted dislocation bow (Fig. 7c gives some examples) is evaluated with the help of a stencil cut from paper. As most of the soft curved dislocation bows are very short (see the dislocations marked with black arrows in Fig. 7c), the accuracy in the determination of  $r$  is low. If, for example, the picture of a dislocation bow has a true radius of 70 nm, the measured value lies between about 50 and 100 nm. As the possible scattering of values due to errors in the determination of  $r$  is smaller than the true differences between individual dislocations, it was tolerated.

Some problems may also arise in connection with the stability of dislocation bows. Only dislocations which are pinned throughout their whole length on an atomic scale (not only in discrete pinning points) will

keep their position when the specimen is unloaded. Otherwise dislocation bows shorten because of a reduction in line energy. The pinning effect can be obtained with radiation damage. Usually TEM investigation on pure metals is done without pinning; therefore, normally no strong curved dislocation can be found. Working with alloys has the advantage that, if there is a strong affinity between dislocations and foreign atoms, Cottrell clouds will build which hinder the speedy unbowing of dislocations. Therefore, cooling under load may conserve the original arrangement of dislocations.

Another problem of transmission electron microscopy is the preparation of thin foils. In almost all cases (except sometimes with *in situ* high-voltage electron microscopy [21]), the useful thickness of TEM foils is much smaller than the subgrain size. Removing the subgrain walls from the surface of the foil leads to a dramatic change in the distribution of local stresses, which may cause soft pinned dislocations (in alloy-hardened material) to escape or to straighten.

Fig. 8 shows the results of local stress measurements on various specimens deformed at temperatures between 500 and 750 °C. Owing to the uncertainty in  $\alpha$  (see Equation 3) Fig. 8 has two alternative ordinates and two lines where  $\sigma_l$  is equal to  $\sigma$ . In the following discussion and for plotting  $\sigma_e$  values obtained with transient dip tests,  $\alpha$  was set to 0.5 because it would not make any difference in principle, if  $\alpha = 1$ . The highest values obtained from two to four transmission electron micrographs in the subgrain or cell interior of

a specimen are shown for the conventional material ( $\times$ ) or the modified material ( $\blacksquare$ ). As the range of measured local stresses extends to very small values (due to soft curved dislocations visible in most micrographs), a line continues to the smallest stresses evaluated from one specimen. The distribution of the measured values of each specimen is indicated by short thin lines drawn perpendicular to the main line, which is connecting the highest and the smallest measured values. A large density of small lines shows that there is an accumulation of local stresses of individual dislocations.

The large range of local (effective) stresses evaluated in the subgrain interior may have several reasons. One of them may be the recovery of dislocation structures during the cooling and the preparation of thin foils. This generally lowers local internal stresses and therefore increases  $\sigma_e$ , which causes an increase in the curvature of dislocations. Although this possibility cannot be excluded, it is assumed to be not the main reason for strong curved dislocations in the subgrain interior. On the contrary, the distribution of individual, temporarily immobile dislocations inside the subgrains influences the local stresses. These forest dislocations give rise to short-range internal stresses (of different sign) which add to the long-range stresses resulting from the subgrain boundaries. Therefore, a very complex distribution of local stresses will build and, as a consequence, different dislocation curvatures can be found. The mean effective stress acting in the soft regions can be evaluated as an average of a large

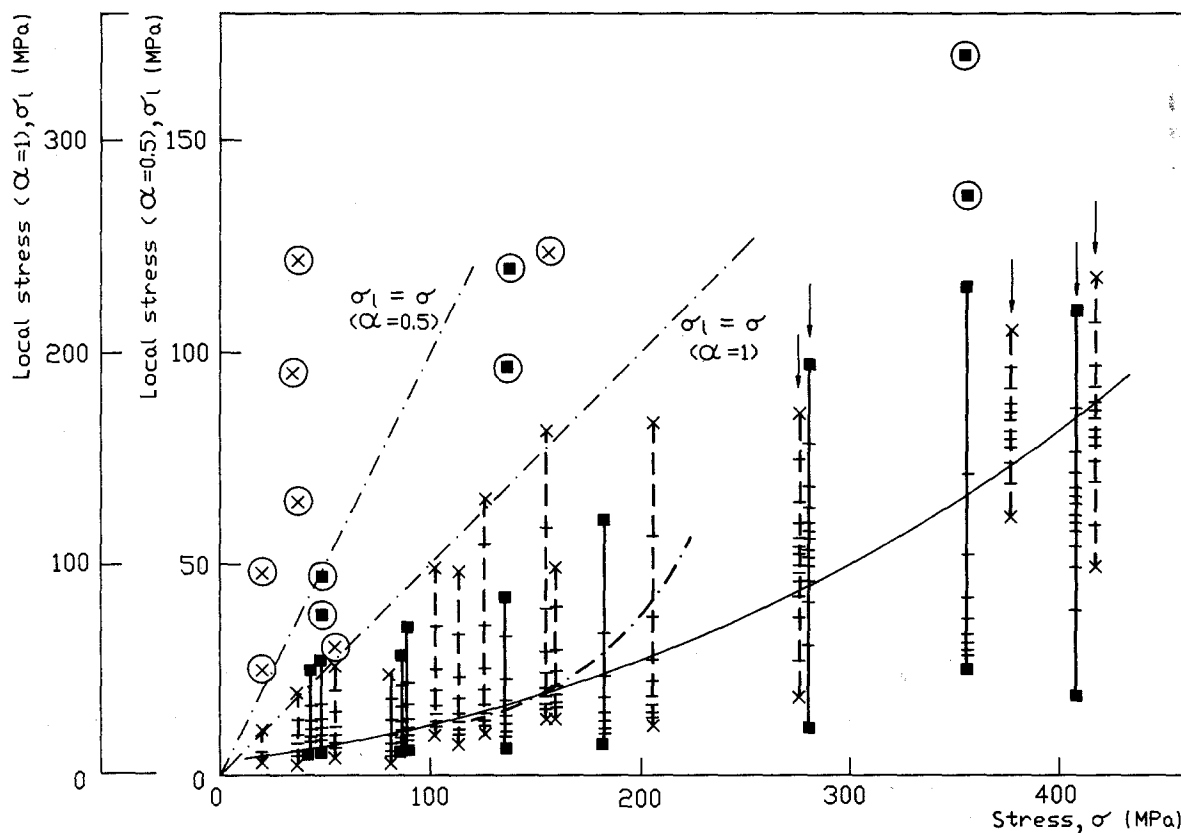


Figure 8 Local stresses evaluated from dislocation bowing in a deformed specimen. Thick vertical lines represent the range of local effective stresses measured for one specimen. A high density of thin short horizontal lines indicates the point at which the majority of individual values lies. For comparison, the results, obtained with stress transient dip tests are shown (—, for  $\alpha = 0.5$ ), (---) conventional material, (—■—) modified material, (—) mean effective stress of dislocation bowing. See also text.

number of dislocations within the subgrain or cell interior, taking into account the distribution of soft and hard curved dislocations.

The evaluation of local stresses presented in Fig. 8 shows some interesting facts. First it can be seen that the local effective stresses in the subgrain interior (all points without surrounding circle) increase with increasing applied stress. This is consistent with the results of stress transient dip tests. Compared to the results of dip tests, the mean effective stress evaluated from dislocation bowing (—, drawn more or less arbitrarily by taking into account the distribution of soft and strong curved dislocations in the subgrain interior) shows a less steep increase. This may be a consequence of mixing values from specimens deformed at different temperatures. It is assumed that the internal stress is lower at high temperatures, even if the same stress is applied [8]. But because of a large range of local stresses within one specimen, the influence of temperature was not excluded. Owing to these uncertainties in the evaluation of a mean value of effective stresses from dislocation bowing, it is clear that this method is only useful to obtain principal information about stress distribution. It cannot be used, however, in cases where highly accurate  $\sigma_e$  values are necessary (e.g. for the determination of the effective stress exponent of dislocation motion,  $m$ , see [22]).

The local stresses in the vicinity of subgrain boundaries are larger than in the subgrain interior and sometimes even larger than the applied stress. This is consistent with the well-accepted theory of Nix and Ilshner [2], which is shown schematically in Fig. 6.

It is interesting to note that only at low applied stresses (up to about 50 MPa) are local stresses in the subboundaries higher than the applied stress. This may be due to a breakdown of the alloying effect with high effective stresses acting on the dislocations. It is shown elsewhere [17, 22] that the interaction between alloying atoms (aluminium and chromium) and dislocations ceases at applied stresses above approximately 450 MPa for aluminium and 220 MPa for chromium. This is a consequence of large effective stresses which cause fast dislocation motion and thus breakaway from Cottrell clouds. Data obtained by the authors indicate an effective stress of about 150–180 MPa for the breakaway of dislocations because no stronger curved dislocation could be found, see Fig. 8. This value may, however, be influenced by the preparation of TEM foils and the evaluation of dislocation curvature. Further work with *in situ* high-voltage electron microscopy should be done.

In the case of the cell walls which are developing in the exponential creep region [6, 7], the dislocations within the wall are arranged with less order. As the degree of order of the dislocation within the walls changes, the distribution of the local stresses will change too. This means that the peak of local stresses will become less sharp and the relative height of the stress peak will decrease. As a consequence also, the normalized long-range internal stresses,  $\sigma_i/\sigma$ , in the regions with low dislocation density, decrease, and thus  $\sigma_e/\sigma$  increases. This is shown by the mechanical

measurements (dip tests), Fig. 5, and by the TEM analysis of dislocation structure, Fig. 8.

#### 4. Conclusions

The ferritic chromium steel X10CrAl 18 was tested in two structural conditions in a temperature range 500–750 °C and at strain rates between  $2 \times 10^{-7}$  and  $2 \times 10^{-2} \text{ s}^{-1}$ . Stress transient dip tests, which were applied only at a temperature of 600 °C, show that

1. the increase of internal stress becomes small or ceases in the vicinity of the transition to exponential creep; and

2. the ratio of  $\sigma_i/\sigma$  decreases from about 0.85 to 0.75 when the stress increases from 150 to 210 MPa. There are only small differences between two structural conditions of the investigated alloy, which differ in grain and carbide size, as well as carbide distribution.

The results of local stress measurements with dislocation curvature observed in transmission electron micrographs show that

3. the local effective stresses increase with the applied stress;

4. measurements of local stresses are valuable only for comparison because there are many influences which can alter the dislocation arrangement during unloading of the specimen and during preparation of the TEM foil. On the other hand, true alternations of local effective stresses are caused by the statistic distribution of dislocations within the low-density regions. This presents some difficulties in finding the mean value of effective stresses.

5. in the vicinity of subgrain boundaries the local internal stresses are higher than in the subgrain interiors and sometimes also higher than the applied stress. This result fits well with the creep theory of “hard” and “soft” zones which was introduced by Nix and Ilshner [2]. The fact that no local effective stress higher than approximately 150–180 MPa could be found, may be interpreted in terms of breakaway of dislocations from their Cottrell clouds.

#### Acknowledgement

The financial support granted by the “Fonds zur Förderung der wissenschaftlichen Forschung in Österreich” is gratefully acknowledged (Project no. 5574).

#### References

1. W. BLUM, *Z. Metallkde* **68** (1977) 484.
2. W. D. NIX and B. ILSCHNER, in “Proceedings of the 5th International Conference on the Strength of Metals and Alloys”, Vol. 3, Aachen, August 1979, edited by P. Haasen, V. Gerold and G. Kostorz (Pergamon, Oxford, 1979) p. 1503.
3. H. J. FROST and M. F. ASHBY, in “Deformation Mechanism Maps, The Plasticity and Creep of Metals and Ceramics” (Pergamon, Oxford, 1982).
4. D. CAILLARD, *Mater. Sci. Engng* **81** (1986) 349.
5. M. BIBERGER and W. BLUM, *Scripta Metall.* **23** (1989) 1419.
6. F. GROISBÖCK and R. EBNER, *Z. Metallkde*, **82** (1991) 435.

7. F. GROISBÖCK, Doctoral thesis, Leoben (1990).
8. S. TAKEUCHI and A. S. ARGON, *J. Mater. Sci.* **11** (1976) 1542.
9. F. GROISBÖCK, R. EBNER and F. JEGLITSCH, in "Proceedings of the 1st International Conference on Advanced Materials and Processing", Aachen, November 1989, edited by H. E. Exner and V. Schumacher (DGM Informationsgesellschaft mbH, Oberursel, 1990), p. 579.
10. J. CADEK, *Mater. Sci. Engng* **94** (1987) 79.
11. S. U. AN, H. WOLF, S. VOGLER and W. BLUM, in "Proceedings of the 4th International Conference on Creep and Fracture of Engineering Materials and Structures", Swansea, April 1990, edited by B. Wilshire and R. W. Evans (Institute of Metals, London, 1990), p. 81.
12. A. A. SOLOMON, *Rep. Sci. Instrum.* **40** (1969) 1025.
13. C. N. AHLQUIST and W. D. NIX, *Scripta Metall.* **3** (1969) 679.
14. J. J. URCOLA and C. M. SELLARS, *Acta Metall.* **35** (1987) 2659.
15. K. TOMA, H. YOSHINAGA and S. MOROZUMI, *Trans. Jpn Inst. Metals* **17** (1976) 102.
16. W. BLUM and E. WECKERT, *Mater. Sci. Engng* **86** (1987) 145.
17. F. GROISBÖCK and R. DANZER, *Z. Metallkde.* **82** (1991) 519.
18. F. DOBES, *Acta Metall.* **28** (1980) 377.
19. J. FRIEDEL, in "Dislocations" (Addison Wesley, Reading, MA, 1964), Ch. 16.
20. J. FRIEDEL, in "Electron Microscopy and Strength of Crystals", edited by G. Thomas and J. Washburn (Interscience, 1963) p. 605.
21. L. P. KUBIN and J.-L. MARTIN, in "Proceedings of the 5th International Conference on the Strength of Metals and Alloys", Vol. 3, Aachen, August 1979, edited by P. Haasen, V. Gerold and G. Kostorz (Pergamon, Oxford, 1979) p. 1639.
22. F. GROISBÖCK, *J. Mater. Sci.* **27** (1992) 4373.

*Received 12 April  
and accepted 7 October 1991*